AIP | Applied Physics Letters

InAs-based interband-cascade-lasers emitting around 7 μm with threshold current densities below 1 kA/cm2 at room temperature

Matthias Dallner, Florian Hau, Sven Höfling, and Martin Kamp

Citation: Applied Physics Letters **106**, 041108 (2015); doi: 10.1063/1.4907002
View online: http://dx.doi.org/10.1063/1.4907002
View Table of Contents: http://scitation.aip.org/content/aip/journal/apl/106/4?ver=pdfcov
Published by the AIP Publishing

InAs-based interband-cascade-lasers emitting around 7 μm with threshold current densities below 1 kA/cm^2 at room temperature

Matthias Dallner,[1] Florian Hau,[1] Sven Höfling,[1,2] and Martin Kamp[1]
[1]*Technische Physik, University of Würzburg, 97074 Würzburg, Germany*
[2]*SUPA, School of Physics and Astronomy, University of St. Andrews, St. Andrews KY16 9SS, United Kingdom*

(Received 15 December 2014; accepted 19 January 2015; published online 28 January 2015)

Interband cascade lasers (ICLs) grown on InAs substrates with threshold current densities below 1 kA/cm^2 are presented. Two cascade designs with different lengths of the electron injector were investigated. Using a cascade design with 3 InAs quantum wells (QWs) in the electron injector, a device incorporating 22 stages in the active region exhibited a threshold current density of 940 A/cm^2 at a record wavelength of 7 μm for ICLs operating in pulsed mode at room temperature. By investigating the influence of the number of stages on the device performance for a cascade design with 2 QWs in the electron injector, a further reduction of the threshold current density to 800 A/cm^2 was achieved for a 30 stage device. © *2015 AIP Publishing LLC*.
[http://dx.doi.org/10.1063/1.4907002]

Efficient and reliable laser sources in the mid-infrared spectral region are crucial for a variety of applications, such as tunable laser absorption spectroscopy (TLAS). The vast improvements in the performance of interband cascade lasers (ICLs)[1] over the last years have made this laser type a promising candidate for these tasks. ICLs grown on GaSb-substrates have proven capable of covering wavelengths from around 3 μm up to 5.6 μm in room temperature cw operation.[2–5] InAs-based ICLs allowed a further extension of the covered emission wavelengths up to 10.4 μm at cryogenic temperatures.[6–8] Here, a plasmon waveguide configuration is used instead of superlattice claddings for an easier growth and better thermal conductivity.[9] While injector-based quantum cascade lasers (QCLs) have already shown cw operation at room temperature with high output powers in this wavelength region,[10,11] they suffer from relatively high threshold power densities due to the short upper state lifetimes and the resulting need for a large number of cascades to generate sufficient gain. However, a 60 stage injectorless QCL device emitting at 6.8 μm was able to show a threshold power density below 6 kW/cm^2 at 300 K.[12] In this work, we present InAs-based ICLs with threshold current densities (j_{th}) in pulsed operation below 1 kA/cm^2, threshold power densities below 10 kW/cm^2, and emission wavelengths around 7 μm. It is worth mentioning that, in addition to the achievement of a long wavelength room temperature emission record for ICLs, these pulsed threshold current density values are the lowest at room temperature reported so far for InAs-based ICLs.

The samples presented in this work were grown using an EIKO molecular beam epitaxy system on n-type InAs substrates. For the group III elements, normal solid source effusion cells were used while cracker cells were used for the group V elements arsenic and antimony. A growth temperature of 450 °C, measured by a pyrometer, was maintained throughout the growth for all InAs-layers, including the waveguide and cladding layers. No temperature adjustments were made for the AlSb, GaSb, and GaInSb layers in the active region. As all layers used in the structure are either lattice matched or compressively strained with respect to the InAs substrate, there is no strain compensation by the layers itself as in GaSb-based ICLs. In order to at least partially compensate the compressive strain, highly tensile strained AlAs interfaces are favorable at the InAs/AlSb transitions. For this reason, we included growth interruptions of 6 s under As flux after the AlSb barriers in the electron injector to enforce AlAs interfaces. No growth interruptions were added within the W-quantum well (QW) or the hole injector.

Two active region designs were used in this work, as illustrated in Figure 1. Design A is similar to the one reported in Ref. 8, with a short electron injector containing three InAs QWs. Minor changes were necessary regarding the QW widths in the active region to extend the emission wavelength to 7 μm. The total layer sequence of one cascade is 2.5 nm AlSb/4.55 nm InAs/1.2 nm AlSb/3.5 nm InAs/1.2 nm AlSb/3.4 nm InAs/2.5 nm AlSb/3.15 nm InAs/3.0 nm $Ga_{0.76}In_{0.24}Sb$/2.75 nm InAs/1.0 nm AlSb/3.0 nm GaSb/1.0 nm AlSb/4.5 nm GaSb/2.5 nm AlSb. The first and second InAs-QW in the electron injector are Si-doped with a concentration of 1×10^{18} cm^{-3} to achieve carrier rebalancing within the W-QW[4] and hence improve the device performance. Design B features an even shorter electron injector, containing only two InAs/AlSb pairs. The W-QW and the hole injector sequences are left unchanged. The layer sequence for this design is 2.5 nm AlSb/4.35 nm InAs/1.2 nm AlSb/3.3 nm InAs/2.5 nm AlSb/3.15 nm InAs/3.0 nm $Ga_{0.76}In_{0.24}Sb$/2.75 nm InAs/1.0 nm AlSb/3.0 nm GaSb/1.0 nm InAs/4.5 nm GaSb/2.5 nm AlSb. Both InAs-QWs in the electron injector were again Si-doped at 1×10^{18} cm^{-3}. General benefits expected from a shortened injector design are slightly increased mode intensities in the active region[13] and hence a higher gain, and less hetero-interfaces.

The number of cascades was increased with respect to Ref. 8 to compensate for the increased losses at longer wavelengths, as well as the reduced spatial overlap of the electron and hole wavefunctions in the W-QW. The latter is reduced from 23.6% to 21.0% by shifting the wavelength from 6 μm to 7 μm. For both designs, samples with 22 cascades in the active region were fabricated, named as A22 and B22. To

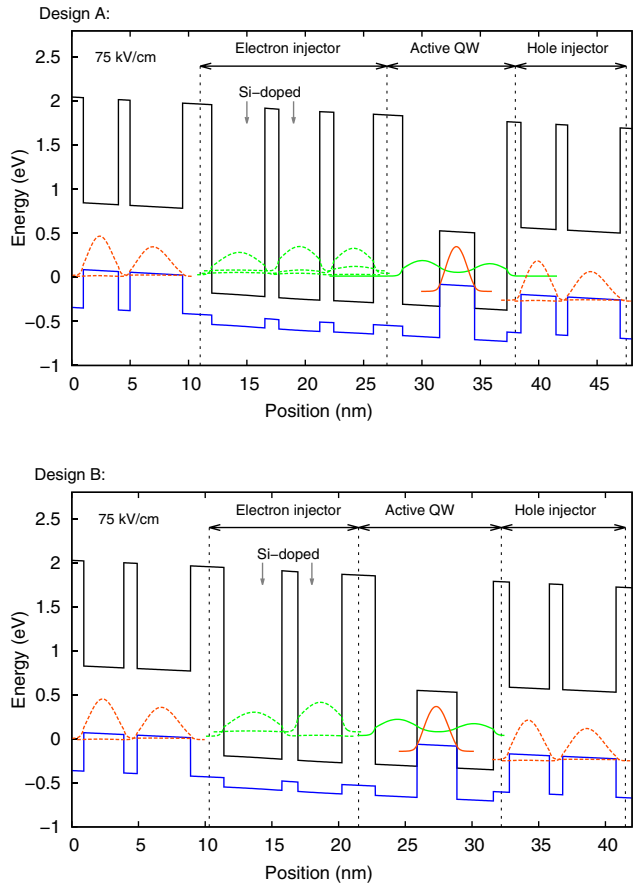

FIG. 1. Simulations of a cascade structure of designs A and B, containing the electron and hole injectors and the active W-QW. The black lines indicate the conduction band edge, the blue curve indicates the heavy hole band edge. The electron and hole probability densities are represented by the green and orange curves, respectively. An electric field of 75 kV/cm was used for both simulations.

study the influence of the cascade number on the device performance, additional samples with stage design B were grown with 18, 26, and 30 cascades, named as B18, B26, and B30, respectively.

The active region of each laser was embedded in thick undoped InAs layers with equal widths on top and bottom acting as waveguide. The nominal width of these layers was 1290 nm for samples A22 and B22 with 22 cascades in the active region. For the samples B18, B26, and B30, waveguide widths of 1370 nm, 1210 nm, and 1130 nm were chosen, respectively, to keep the same mode overlap with the cladding region, and hence constant absorption losses in this region for all samples. 1600 nm thick cladding layers consisting of highly Si-doped InAs with a doping concentration of $3 \times 10^{19}\,\mathrm{cm}^{-3}$ provide the refractive index contrast required for a proper mode confinement. All layers of the waveguide structure were grown epitaxially with a growth rate of 890 nm/h, resulting in a total thickness of the grown layers of around 6.5 μm.

After growth, the samples were processed into ridge waveguide lasers. An inductively coupled plasma reactive ion etch step was used to etch the structures to a depth of around 4.0 μm through the active region into the bottom waveguide, followed by a short wet etch using phosphoric acid to clean the surface. Afterwards, 200 nm Si_3N_4 and 200 nm SiO_2 passivation layers were sputtered on the sidewalls to avoid leakage currents. The samples were then cleaved into laser bars of defined length. No facet treatment was applied and the devices were measured epi-side up on a copper heatsink. To minimize the heating of the samples during the measurement, the devices were measured in pulsed mode at a pulse frequency of 1 kHz and a pulse width of 100 ns.

Figure 2 shows the pulsed light-current characteristics of sample A22 at several temperatures between 0 °C and 50 °C. The measured device was 2 mm long and 45 μm wide. The threshold current density at 20 °C is 940 A/cm^2. The reduced j_{th} with respect to our previous results from Ref. 8 is mainly a consequence of the higher doping in the active region for carrier rebalancing and the increased number of cascades. Below 40 °C, a T_0 value of 35 K was extracted from the measurements, with a reduced value of 13 K above this temperature up to the maximum operation temperature of 55 °C. The set-in voltage at 20 °C, extracted from an extrapolation of the voltage-current curve to I = 0 A, is 5.9 V. Comparing this to the theoretical minimum set-in voltage of 4.0 V, which is given by the product of the photon energy and the number of cascades, this indicates parasitic voltage drops of around 86 mV per stage. For the threshold power density, a value of 7.2 kW/cm^2 was extracted. Figure 3 shows emission spectra of this device at temperatures of 0 °C, 20 °C, and 40 °C. Emitting at a wavelength of 7 μm at 20 °C, this is the longest wavelength ICL working at room temperature reported so far. A temperature induced wavelength tuning rate of approximately 4.8 nm/K was found, which is higher than the value of 3.2 nm/K reported elsewhere for ICLs in this wavelength region at cryogenic temperatures.[14]

For sample B22, a slightly increased j_{th} of 1100 A/cm^2 was measured at 20 °C in pulsed operation for a device with equal dimensions. As is shown by the exponential fits to the measurement data in Figure 4, the T_0 value below 35 °C is 30 K, and 10 K above this temperature. Lasing operation could be maintained up to a temperature of 43 °C. Hence, the longer cascade structure of design A shows superior results in terms of the threshold current density. This might be caused partly by increased losses due to the close vicinity of the doped layers to the W-QW in design B, whereas an

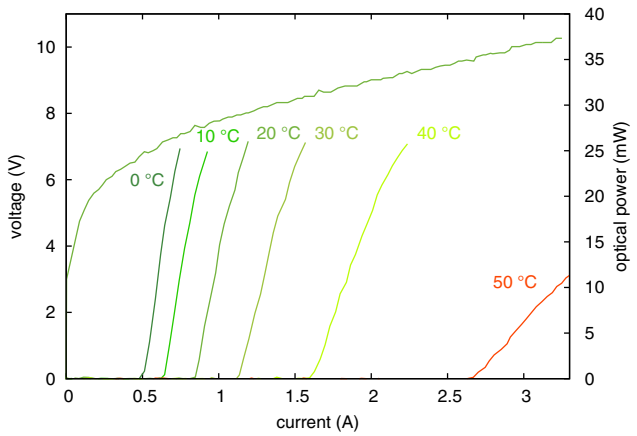

FIG. 2. Light-current characteristics at several temperatures between 0 °C and 50 °C of a 2 mm long and 45 μm wide device of sample A22. The voltage-current curve was measured at 20 °C.

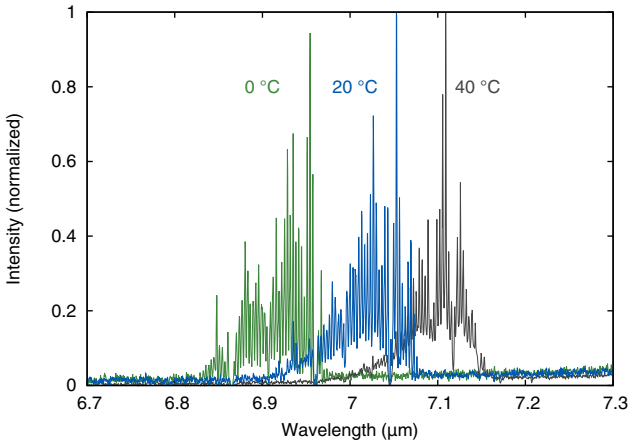

FIG. 3. Emission spectra at 0 °C, 20 °C, and 40 °C of a deeply etched 2 mm long and 45 μm wide device of sample A22. The measurements show a tuning rate of approximately 4.8 nm/K for this device.

undoped InAs QW separates these regions in design A. Hence, an improved performance of design B might be achieved in future devices by optimizing the doping profile. The set-in voltage of device B22 is 5.1 V, meaning lower parasitic voltage drops in the active region as for sample A22. However, the higher threshold current density still results in a slightly higher threshold power density of 7.9 kW/cm^2 compared to sample A22.

Figure 4 also shows the temperature dependent threshold current densities of samples B18, B26, and B30 with a variation of the cascade numbers. In general, the threshold current density is expected to decrease with increasing cascade numbers, as the overall device gain is increased. At the same time, however, due to the series connection of the cascades, the threshold voltage is expected to increase, as the voltage drop in the active region scales linearly with the number of cascades. Hence, the lowest value of the threshold power density depends on the actual dependence of those two parameters. The dependence of j_{th} and the threshold power density on the number of cascades at 20 °C is shown in Figure 5. A steady decrease in j_{th} can be observed with values of 1160 A/cm^2 (B18), 1110 A/cm^2 (B22), 930 A/cm^2

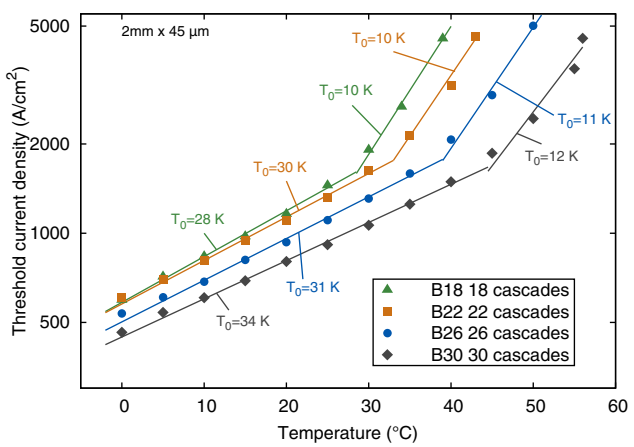

FIG. 4. Temperature dependent threshold current densities for samples B18 to B30. Each laser was 2 mm long and 45 μm wide. The straight lines represent exponential fits of the measured data to retrieve the T_0 values of each device.

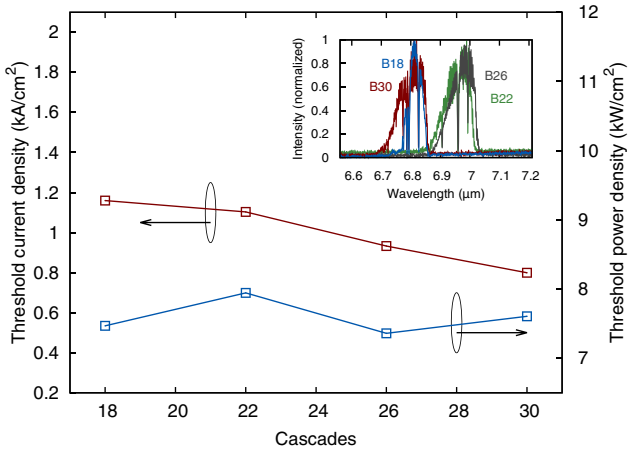

FIG. 5. Threshold current densities (red) and threshold power densities (blue) of 2 mm long and 45 μm wide deeply etched devices of samples B18 (18 cascades), B22 (22), B26 (26), and B30 (30). The inset shows the emission spectra of these devices at 20 °C.

(B26), and 800 A/cm^2 (B30), meaning a further reduced threshold current density with respect to sample A22. The latter is the lowest pulsed threshold current density at room temperature reported for InAs-based ICLs so far. For the set-in voltage, values of 4.7 V, 5.1 V, 5.4 V, and 7.3 V were retrieved for samples B18, B22, B26, and B30, respectively. The resulting threshold power densities do not show a clear trend along the cascade numbers. The lowest value was determined for device B26 at 7.3 kW/cm^2, which is slightly higher than that for device A22. The T_0 values slightly increase with the number of cascades. Values of 28 K, 30 K, 31 K, and 34 K were retrieved for samples B18, B22, B26, and B30, respectively, around 20 °C. The wavelengths for the devices at 20 °C vary slightly between 6.80 μm and 6.95 μm as can been seen in the inset of Figure 5.

We have shown ICLs grown on InAs substrates with two different active region designs. Lasers from both designs were able to emit around 7 μm with threshold current densities below 1 kA/cm^2, although the design with a longer electron injector showed superior results with regard to the threshold current density and threshold power density at equal stage counts. By increasing the cascade numbers, a steady decrease in threshold current density was found, resulting in a record low threshold current density of 800 A/cm^2 for a device with 30 cascades and a short electron injector containing 2 QWs. A threshold power density of 7.2 kW/cm^2 was found for a device comprised 22 stages and the injector design with 3 QWs.

We acknowledge the financial support from the European Commission in the frame of the FP7 project "WideLase" (Grant No. 318798). We also would like to thank A. Wolf, M. Wagenbrenner, and S. Kuhn for assistance during sample preparation, growth, and characterization and R. Weih for fruitful discussions. S.H. gratefully acknowledges the support by the Royal Society and the Wolfson Foundation.

[1]R. Q. Yang, Superlattices Microstruct. **17**(1), 77 (1995).
[2]W. Bewley, C. Canedy, C. Kim, M. Kim, C. Merritt, J. Abell, I. Vurgaftman, and J. Meyer, Opt. Express **20**, 20894 (2012).

[3]C. L. Canedy, J. Abell, C. D. Merritt, W. W. Bewley, C. S. Kim, I. Vurgaftman, J. R. Meyer, and M. Kim, Opt. Express **22**, 7702 (2014).
[4]I. Vurgaftman, W. W. Bewley, C. L. Canedy, C. S. Kim, M. Kim, C. D. Merritt, J. Abell, J. R. Lindle, and J. R. Meyer, Nat. Commun. **2**, 585 (2011).
[5]R. Weih, M. Kamp, and S. Höfling, Appl. Phys. Lett. **102**, 231123 (2013).
[6]Z. Tian, L. Li, H. Ye, R. Q. Yang, T. D. Mishima, M. B. Santos, and M. B. Johnson, Electron. Lett. **48**(2), 113–114 (2012).
[7]Z. Tian, Y. Jiang, L. Li, R. T. Hinkey, Z. Yin, R. Q. Yang, T. D. Mishima, M. B. Santos, and M. B. Johnson, IEEE J. Quantum Electron. **48**, 915 (2012).
[8]M. Dallner, S. Höfling, and M. Kamp, Electron. Lett. **49**, 286 (2013).
[9]Z. Tian, R. Q. Yang, T. D. Mishima, M. B. Santos, R. T. Hinkey, M. E. Curtis, and M. B. Johnson, Electron. Lett. **45**, 48 (2009).
[10]R. Maulini, A. Lyakh, A. Tsekoun, and C. K. N. Patel, Opt. Express **19**, 17203 (2011).
[11]N. Bandyopadhyay, Y. Bai, S. Slivken, and M. Razeghi, Appl. Phys. Lett. **105**, 071106 (2014).
[12]G. Boehm, S. Katz, R. Meyer, and M.-C. Amann, J. Cryst. Growth **311**, 1932 (2009).
[13]A. Bauer, M. Dallner, M. Kamp, S. Hofling, L. Worschech, and A. Forchel, Opt. Eng. **49**, 111117 (2010).
[14]Z. Tian, R. Q. Yang, T. D. Mishima, M. B. Santos, and M. B. Johnson, IEEE Photonics Technol. Lett. **21**(21), 1588 (2009).